KI REPORTS
KIReports.org
NEPHROLOGY ROUNDS

Tubular Epithelial and Peritubular Capillary Endothelial Injury in COVID-19 AKI

John C. Papadimitriou[1], Cinthia B. Drachenberg[1], David Kleiner[2], Nadia Choudhri[3], Abdolreza Haririan[3] and Valeriu Cebotaru[3]

[1]Department of Pathology, University of Maryland School of Medicine, Baltimore, Maryland, USA; [2]Laboratory of Pathology, Center for Cancer Research, National Cancer Institute, Bethesda, Maryland, USA; and [3]Department of Medicine, Division of Nephrology University of Maryland School of Medicine, Baltimore, Maryland, USA

Correspondence: John C. Papadimitriou, Pathology, University of Maryland Hospital, 22 South Greene Street, NBW71, Baltimore, Maryland 21201, USA. E-mail: jpapadimitriou@som.umaryland.edu

Received 28 August 2020; accepted 27 October 2020; published online 5 November 2020

Kidney Int Rep (2021) **6,** 518–525; https://doi.org/10.1016/j.ekir.2020.10.029

INTRODUCTION

Multiple reports describe respiratory system involvement in coronavirus disease 2019 (COVID-19), but in patients who require hospitalization, concurrent renal dysfunction is common.[1] In a large study, more than 36% of patients developed acute kidney injury (AKI), and of those, 14.3% required renal replacement therapy.[S1] Development of AKI occurs early, is temporally associated with acute respiratory failure, and carries worse overall prognosis.[S1–4]

The etiology of AKI in COVID-19 is considered to be multifactorial, due to volume depletion, poor renal perfusion, sepsis, and systemic inflammatory cytokine storm.[S5] Severe acute respiratory syndrome coronavirus 2 (SARS-CoV-2) renal tropism has been suggested, and significant amounts of viral RNA were detected by polymerase chain reaction in kidney tissue from some patients with viremia.[S6,S7] Conclusive morphological evidence of SARS-CoV-2 viral particles in the renal parenchyma is lacking, although electron microscopy studies have shown abundant intracellular vesicular structures, resembling SARS-CoV-2 viral particles.[2] These structures, most likely representing clathrin-coated transport vesicles,[3] do not fulfill the morphological criteria for corona virions,[S8–S11] but highlight a profound ultrastructural alteration in renal tissue, comparable to that seen in other cell types after oxidative stress injury.[4,5]

In the lung, vascular involvement, including endothelial cell damage, vascular inflammation, thrombosis, and microangiopathy, as well as regeneration with neoangiogenesis, points to the vascular endothelium as an important target of COVID-19.[S7,S8,S12,S13] In the kidney, severe vascular congestion and possible microthrombi were interpreted as evidence of vascular injury[6]; however, systematic ultrastructural evaluation of the renal endothelium in COVID-19 is not available.

CASE PRESENTATION

Case 1

A 52-year-old man with longstanding well-controlled HIV, hypertension, coronary artery disease, and Factor V deficiency presented to the emergency department with severe vomiting and diarrhea for approximately a week, and tested positive with a nasal swab reverse-transcriptase polymerase chain reaction for SARS-CoV-2. He also noted episodes of epistaxis and myalgias, but denied fever, chills, cough, shortness of breath, chest pain, or edema. His blood pressure was 120–140s/80s, and he was not hypoxic. Initial blood urea nitrogen and serum creatinine were 30 mg/dl and 7.5 mg/dl, respectively. Serum creatinine was normal 2 months earlier. Complete blood count was normal, except for mild normocytic anemia. HIV viral load was undetectable and CD4 count was normal. Ferritin level was high (1427 ng/ml, normal 23–336), as were C-reactive protein (109 mg/l, normal <6) and D-dimer (630 ng/ml, normal 0–500). The patient was initiated on intravenous fluids and admitted to the intensive care unit. He was initially alert and conversant, but notably anxious, with no other significant clinical findings. He developed severe epistaxis and subsequently acute hypoxemic respiratory failure requiring intubation and mechanical ventilation on day 2. Imaging studies of the lungs showed pulmonary edema. Piperacillin/tazobactam and hydroxychloroquine were initiated, as well as renal replacement therapy, due to persistent

azotemia. The clinical course was complicated by paroxysmal atrial fibrillation treated with amiodarone, and acute anemia and thrombocytopenia requiring transfusion of red blood cells and platelets. After 48 hours of mechanical ventilation, the patient was extubated and was stable on room air. Gastrointestinal symptoms, including nausea and diarrhea, persisted for a few days. Spot urine protein/creatinine ratio revealed 1.85 g/g proteinuria. C3 and C4 complement components were normal, and serological studies including autoimmune and hepatitis panels were negative. There was no evidence of monoclonal gammopathy. Renal biopsy was performed on day 10 of hospital stay for proteinuria and lack of improvement of the renal function. Nasal swabs for SARS-CoV-2, repeated 7 and 14 days after admission were negative. During and after hospitalization, the patient had improving urine output, but required intermittent hemodialysis. Renal replacement therapy was stopped 11 weeks after the COVID-19 diagnosis.

Case 2

A 64-year-old man with history of atrial fibrillation, on home aspirin, with hyperlipidemia and gout, presented with cough, fever, and chest pain. A nasal swab reverse-transcriptase polymerase chain reaction for SARS-CoV-2 was positive. He was admitted for hypoxemia, and on day 5 was intubated due to worsening hypoxemia. He was started on i.v. heparin anticoagulation for atrial fibrillation and then transitioned to apixaban. His hospital stay was complicated by a large-volume hematemesis and coffee ground emesis requiring 4 units of blood and plasma transfusions and was started on norepinephrine for hypotension. He then developed atrial fibrillation with rapid ventricular response and was started on amiodarone infusion and diltiazem drip. Two attempts at cardioversion were not successful. His sputum grew *Escherichia coli* and he was started on meropenem on hospital day 13. On hospital day 19 the patient was found to have a decreased mental status and had a computed tomography of the head that did not show any acute process.

On day 22, the patient underwent a tracheostomy and on the same day he was started on continuous renal replacement therapy for persistent azotemia and volume removal. On hospital day 29 he was transitioned to intermittent hemodialysis. On hospital day 33, hemodialysis was stopped. He came off ventilator support on day 78. His hospital course was complicated by methicillin-resistant *Staphylococcus aureus* bacteremia treated with linezolid, *Pseudomonas* and *E. coli* ventilator-associated pneumonia treated with i.v. imipenem/cilastatin/relebactam and inhaled colistin and polymyxin B. He also developed a right axillary and right subclavian deep venous thrombosis and was started on i.v. heparin.

Initial laboratory tests revealed blood urea nitrogen 20 mg/dl, creatinine 1.4 mg/dl, white blood cell count 4200/μl, hemoglobin 13.4 g/dl, platelets 131K/μl, international normalized ratio 1.0, aspartate aminotransferase 93 U/l, alanine aminotransferase 83 U/l. His baseline creatinine was 1.0 mg/dl. Blood urea nitrogen and creatinine peaked at 130 mg/dl and 4.31 mg/dl, respectively. D-Dimer peaked at 15,230 ng/ml, C-reactive protein peaked at 31.3 ng/ml, and persistently high ferritin reached 4461.7 ng/ml at day 22 (normal 23–336). Nasal swabs for SARS-CoV-2, 10 and 17 days after admission were negative

On hospital day 81, the patient was found to have 7.4 g/g of protein on urine spot protein-to-creatinine ratio. Twenty four-hour urine collection revealed 4.37 g of proteinuria. Autoimmune and hepatitis serological studies were negative and there was no evidence of monoclonal gammopathy. Renal biopsy was performed on hospital day 84. On biopsy day his blood urea nitrogen and creatinine were 51 mg/dl and 1.58 mg/dl, respectively, with an estimated glomerular filtration rate of 36 ml/min (estimated glomerular filtration rate at admission was >60).

Renal Biopsy Findings

Light Microscopy

Marked and diffuse tubular cell injury was seen in both biopsies, with involvement of all cortical tubular segments. The day 10 biopsy (D10Bx) from patient 1 showed severe diffuse simplification of the tubular epithelium, with marked cytoplasmic blebbing-vacuolization, loss of cell polarity, loss of brush border, and spotty or confluent cell dropout (Figure 1a). There were also prominent protein casts and areas of tubular cell sloughing (Supplementary Figure S1A–D). The day 84 biopsy (D84Bx) from patient 2 showed diffuse tubular injury characterized by cytoplasmic swelling with marked coarse and isometric vacuolization (Figure 1b). Also noted was irregular simplification with partial loss of brush border of the proximal tubules, admixed with hyperplastic and reparative changes in all tubule segments (Figure 1b). Dense protein and cellular casts were noted in both cases (Supplementary Figures S1D and S2A).

The peritubular capillaries (PTC) were prominent in both biopsies. There was peritubular capillary dilatation with endothelial cell nuclear enlargement and luminal protrusion (Figure 1a and b and 2a and d). Interstitial inflammation was sparse on routine stains, but the CD68 immunostain highlighted clusters of monocytes/macrophages, predominantly around and in peritubular capillaries in both biopsies (Figure 2c and

f). CD31 stains for evaluation of the microvasculature showed disturbed and severely diminished staining consistent with rupture or disintegration/lysis of most PTC endothelial cells in the D10Bx (Figure 2b), whereas the stain strongly highlighted the enlarged and prominent endothelial PTC endothelial cell lining in the D84Bx (Figure 2e).

On light microscopy, the glomeruli were essentially normal with only minimal increase in mesangial matrix on the D10BX (Supplementary Figure S1A) and showed perihilar focal segmental glomerulosclerosis (secondary) on the D84Bx (Figure 2b). Chronic changes were insignificant in both biopsies, with the trichrome stain showing only mild interstitial fibrosis and tubular atrophy (approximately 10%–15% of the cortical areas). The arteries were widely patent, and thrombotic/microangiopathic features were absent. Routine immunofluorescence studies including IgG, IgM, IgA, C3, C4, and C1q, as well as immunohistochemical stains for C3d and C4d stain, were negative in both biopsies.

Terminal deoxynucleotidyl transferase dUTP nick end labeling assay (TUNEL) for evaluation of apoptosis showed only rare apoptotic cells (0–4 apoptotic cells per ×400 field) in both biopsies.

In situ hybridization for SARS-CoV-2 spike and nuclear capside RNA (RNAscope) were negative in both biopsies.

Ultrastructural Findings

Tubular epithelial cell injury was extensive in both biopsies, with more prominent sloughing and denudation of the tubular basement membranes seen on the D10Bx (Figure 1c). In both samples, the tubular epithelial cells displayed large areas of cytoplasmic vacuolization with abnormal/disintegrating brush border due to fragmentation or vesiculation of its membranes (Figure 1c and e, Supplementary Figure S3B). Overall, there were extensive vesicular changes with abundant clathrin-coated vesicles admixed with smooth-walled vesicles (Figure 3c, e, f). The mitochondria were markedly abnormal, with a wide range of changes including matrix condensation, or swelling, dissolution of cristae, myelin figure formation, and accumulation of flocculent densities (Figure 3a–d, Supplementary Figure S3A). In addition, the mitochondria displayed marked size variation with numerous small spherical mitochondria (mitospheres) (Figure 3b).[S14] Disarray of the cytoskeleton with accumulation of collapsing bundles of intermediate and thin filaments was noted in the most swollen tubular cells (Figure 3d).[S15]

On electron microscopy, the PTC on the D10Bx showed very severe endothelial injury and/or rupture (Figure 4a and b). The endothelial cell cytoplasmic membranes and the organelles showed marked vesiculation and dissolution. The mitochondria appeared condensed and engulfed by segments of rough endoplasmic reticulum, a feature consistent with autophagy (Figure 4a). On the D84Bx, the PTC were consistently

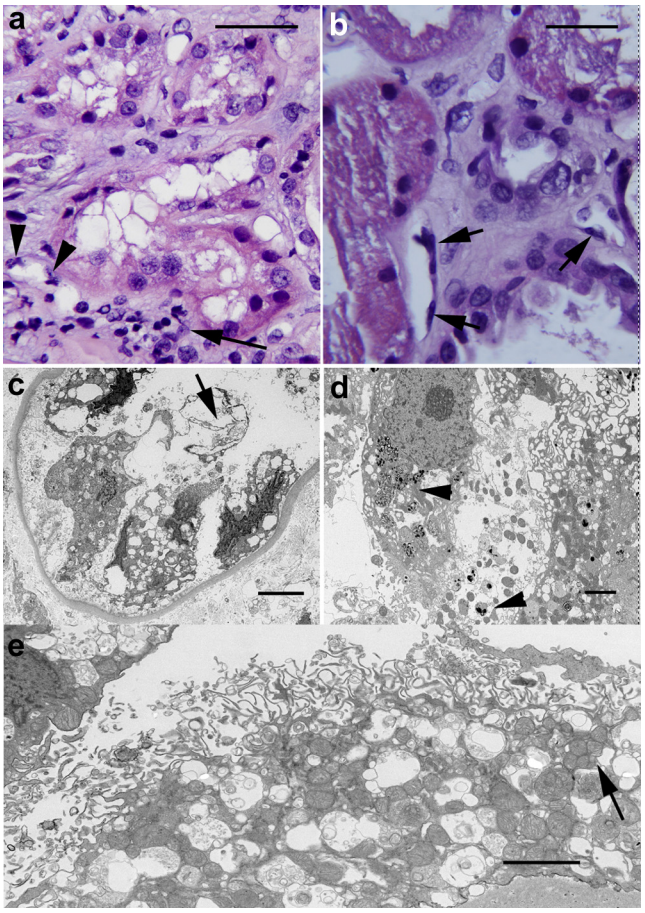

Figure 1. Tubular injury. (a) Day 10 biopsy (D10Bx) tubular epithelium with marked cytoplasmic vacuolization, blebbing, loss of brush border, and spotty cell dropout. The peritubular capillaries (PTC) show endothelial cell changes, including nuclear enlargement and protrusion into the lumen. There is also perivascular and luminal accumulation of mononuclear cells (arrow). Also see Supplementary Figure S2D. (b) Day 84 biopsy (D84Bx) tubular epithelium with diffuse cell injury, cytoplasmic swelling, vacuolization, and blebbing. There is loss of cell polarity, irregular simplification, and loss of brush border admixed with marked reparative changes (center and right). Abnormal PTC endothelial cell lining (arrows) with nuclear enlargement and hyperchromasia. Also see Supplementary Figure S2D. (c) D10Bx electron micrograph of tubule with severe tubular epithelial cell injury with cell sloughing and denudation of the basement membrane. The nuclei appear pyknotic and the cytoplasm severely vacuolated. Fragments of membranes appear in the lumen (arrow). (d) D84Bx, cytoplasmic dissolution and widespread densities consistent with damaged phospholipids suggestive of oxidative membrane injury (arrowheads). The mitochondria appear mostly condensed. (e) D10Bx, disintegration of the brush border and extensive cytoplasmic vesiculation. The mitochondria appear markedly swollen or condensed, with clusters of small mitochondria (mitospheres) (arrow). Bars: (a) and (b) = 25 μm, (c) = 3 μm, (d) and (e) = 2 μm.

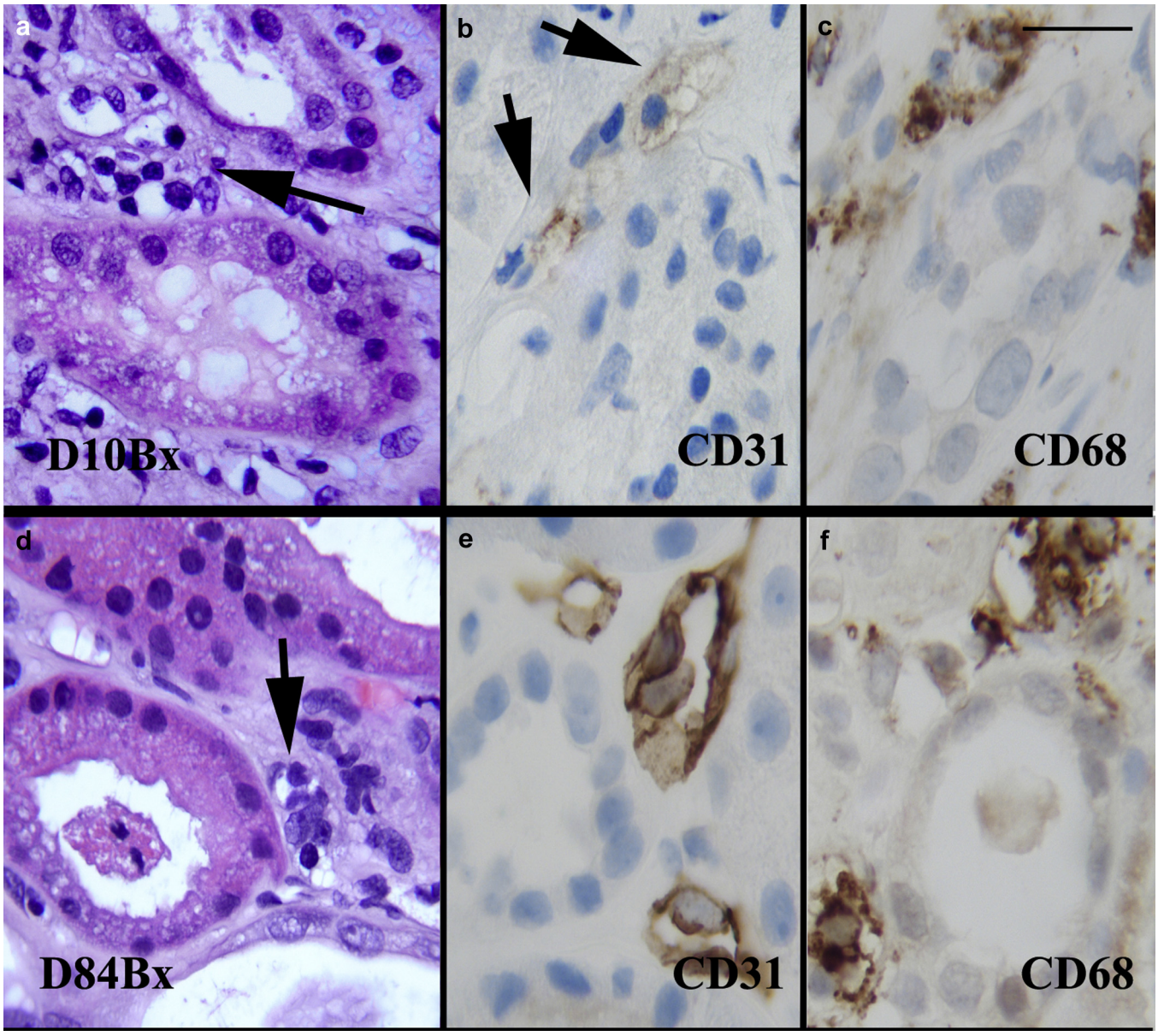

Figure 2. Endothelial injury. Day 10 biopsy: (a) Peritubular capillaries (PTC) (arrow) are prominent due to luminal dilatation, and nuclear enlargement and hyperchromasia of the endothelial cells. There are intraluminal and perivascular mononuclear cell infiltrates. (b) CD31 immunostain is weak and highlights cytoplasmic vesiculation and dissolution of the PTC endothelium (arrows). (c) CD68 immunostain highlights accumulation of macrophages in PTC areas. Day 84 biopsy: (d) PTCs (arrow) are irregularly prominent due to enlargement of the endothelial cell nuclei and increase in mononuclear cells within lumina and surrounding interstitium. The lumina are narrowed in several instances. (e) CD31 highlights the PTC with markedly swollen, hyperplastic endothelial cells. (f) CD68 immunostain highlights macrophages in and around the PTCs. Also see Supplementary Figure S5 for acute kidney injury without features of oxidative stress injury. Bar: (a–f) = 20 μm.

abnormal with swollen or activated appearing endothelial cells and infiltrating monocytes and lymphocytes (Figure 4c and d). The mitochondrial changes were similar to the D10Bx. In addition, there was diffuse, extensive multilamellation of their basal laminae, up to 8 layers (Figure 4e and f), consistent with endothelial cell injury and regeneration.

Glomerular endothelial cells and podocytes showed focal cell swelling and focal accumulation of clathrin-coated or smooth vesicles; however, the foot processes of podocytes were largely preserved in both biopsies (Supplementary Figure S4).

Extensive accumulation of clathrin-coated vesicles with protruding spikes toward the cytoplasm resembling coronavirus in some instances, were observed in both biopsies, but were more prominent in the D10Bx (Figure 3e and f). True viral particles were not identified in either biopsy.

DISCUSSION

COVID-19 may be minimally symptomatic, or present with severe involvement of multiple organ systems. Pneumonia, the most common manifestation of SARS-

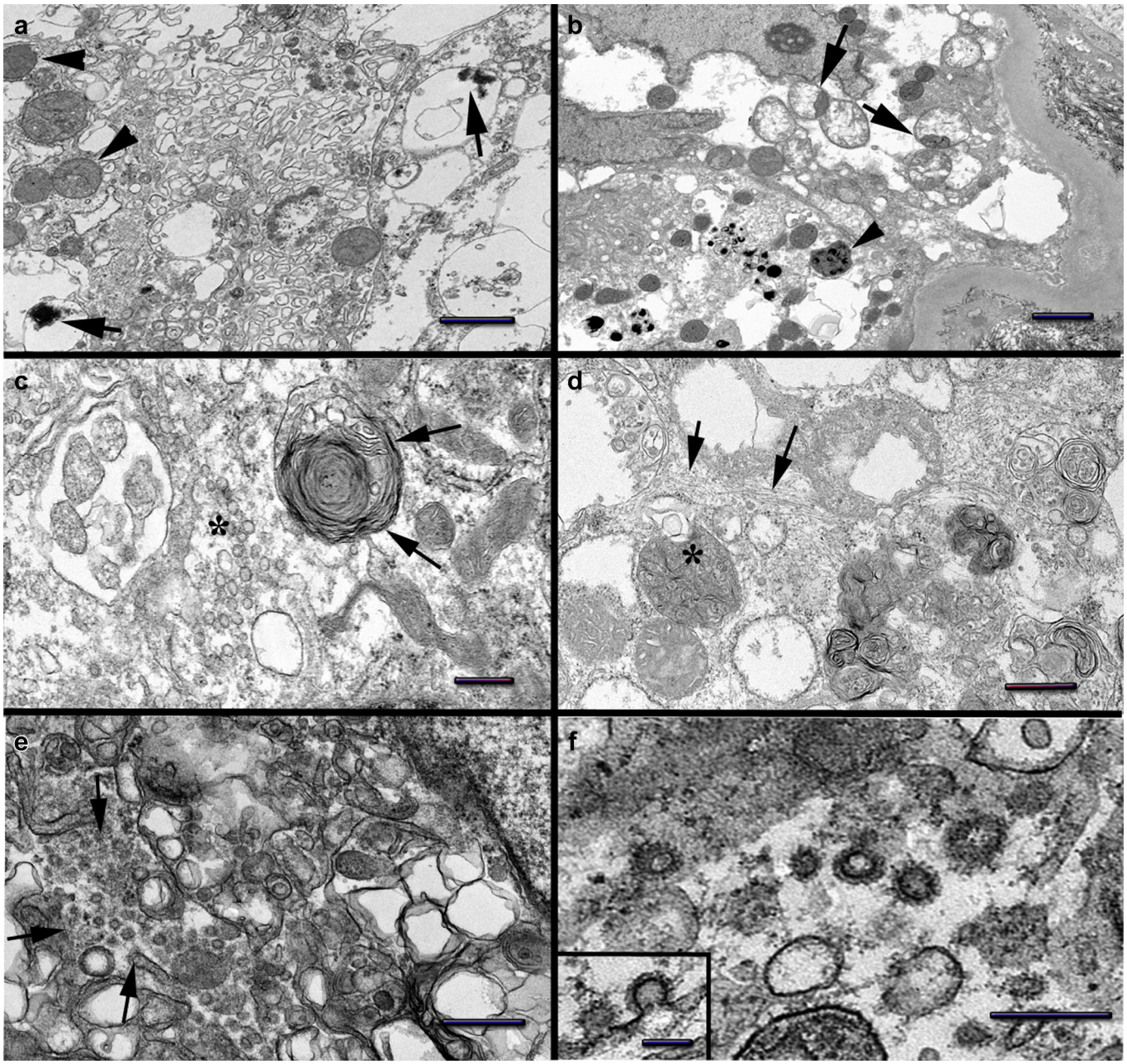

Figure 3. Tubular epithelial cell changes. (a) Day 10 biopsy (D10Bx) tubular epithelial cell shows marked cytoplasmic membrane vesiculation: large vacuoles with densities also seen (arrows). Condensed mitochondria (arrowheads). (b) Day 84 biopsy (D84Bx) marked mitochondrial swelling and/or condensation, occasionally both within the same mitochondrion (segmentation, arrows). Occasional small mitochondria (mitospheres) also noted. Flocculent densities present in rare mitochondria (arrowhead). (c) D10Bx marked vesiculation of the cytoplasm including small smooth-walled vesicles (asterisk) and a multivesicular body to the left. A large myelin figure (arrows) located in the vicinity of atypically shaped condensed mitochondria. (d) D84Bx marked myelin figure formation including myelin containing mitochondria (asterisk). Cytoskeletal filament collapse noted (arrows). (e) D10Bx tubular cells show marked vesiculation of the cytoplasm, including large vesicles and abundant clathrin-coated vesicles resembling viral particles (arrows). (f) D10Bx, tubular epithelial cell cytoplasm with large numbers of vesicles coated by clathrin resembling coronavirus spikes. Insert: Clathrin-coated invagination of the plasma membrane. Bars: (a, d) = 1 μm, (b) = 2 μm, (c) = 400 nm, (e) = 600 nm, (f) = 300 nm (insert = 100 nm).

CoV-2 infection, occurs after engagement of the virus with the angiotensin-converting enzyme 2 receptor expressed in type II pneumocytes. An abundance of angiotensin-converting enzyme 2 receptors in other cell types, including renal tubular cells, enterocytes, and endothelial cells, can explain some of the other manifestations of COVID-19.[S16] Several studies have pointed to the vascular endothelium as an important target of COVID-19 pathophysiology in several organs (e.g., heart and lung).[S8,S12] Endothelial injury in these circumstances can lead to recruitment of immune cells, complement activation, and potentially thrombosis.[S17]

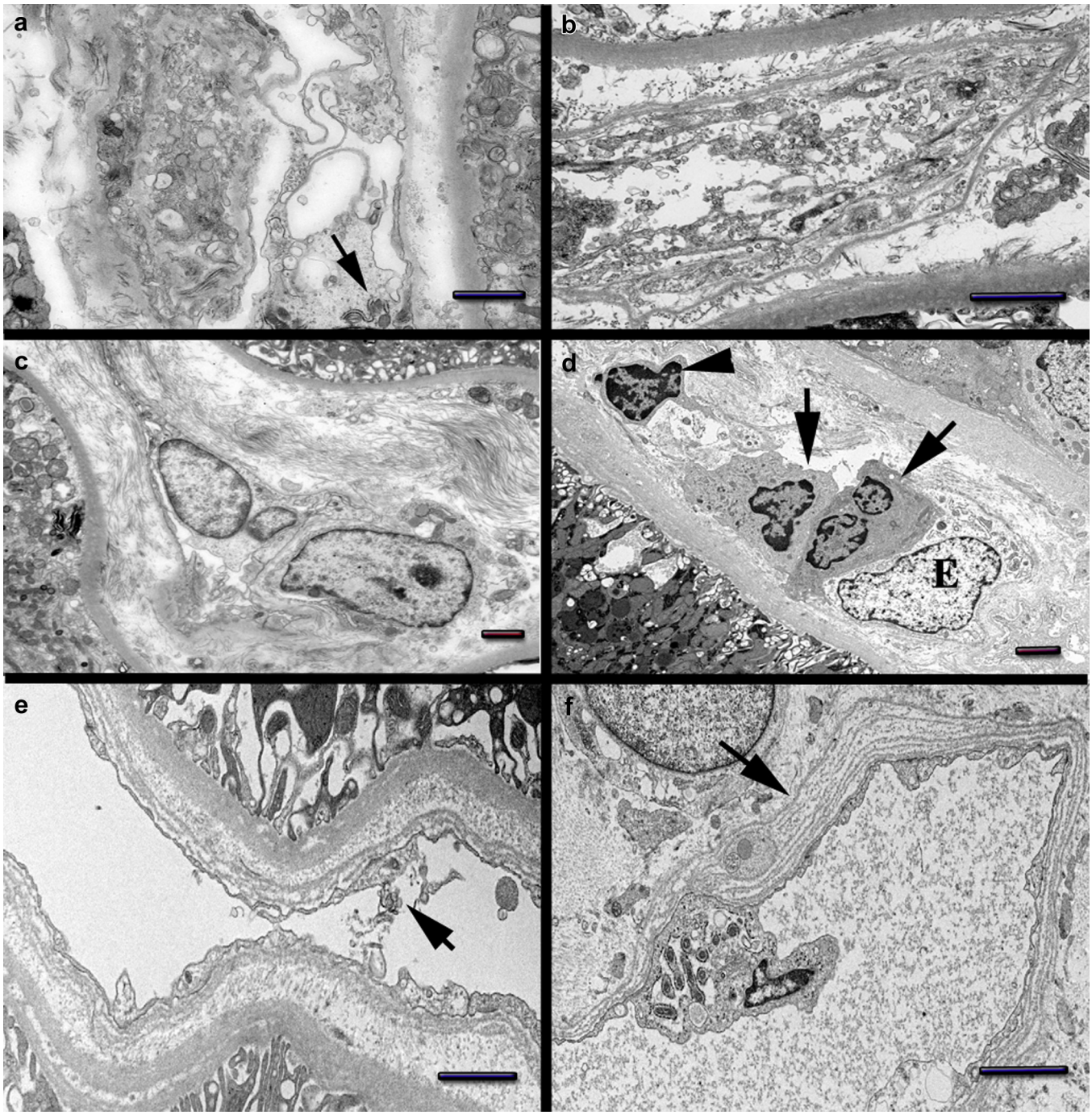

Figure 4. Endothelial cell changes. Day 10 biopsy: (a) Peritubular capillaries (PTC) endothelial cell with marked cytoplasmic vesiculation/dissolution. Condensed mitochondria wrapped by segments of rough endoplasmic reticulum (arrow). (b) PTC endothelial cell with marked membrane injury and massive vesiculation. Abundant cellular fragments shedding into the lumen. Day 84 biopsy: (c) PTC with swelling and hypertrophy of endothelial cells. (d) PTC with swollen endothelial cell (e). The lumen is distended by monocytes (arrows) and a lymphocyte (arrowhead). (e) PTC with fragmented endothelial cell lining (arrow). The basal lamina is multilamellated. (f) Segment of peritubular capillary wall with marked basal lamina multilamellation (arrow). An abnormal endothelial cell protrudes toward the lumen showing rough endoplasmic reticulum wrapping mitochondria suggestive of autophagy. Bars: (a, e, and f) = 1 μm, (b, c, and d) = 2 μm. Also see Supplementary Figure S5 for acute kidney injury without oxidative stress injury.

Renal involvement in the form of AKI carries worse prognosis in COVID-19, and is an increasingly recognized complication in patients with severe disease and in patients with preexisting conditions.[S2,7,S18–S21] In addition to AKI, 40% of the patients have 2 to 3+ proteinuria, leukocyturia, and/or hematuria.[S1]

Severe multiorgan involvement in COVID-19 is generally attributed to a dysregulated host response, initially triggered by innate immune mechanisms on encounter with the virus. An aggressive and exaggerated hyperinflammatory reaction leads to ongoing release of proinflammatory mediators, including

Table 1. Teaching points

AKI is common in the more severe forms of COVID-19, but renal biopsies are rarely performed.
Histopathology shows, in addition to diffuse severe tubular injury, marked injury of the endothelium in peritubular capillaries.
The ultrastructural features in both epithelial and endothelial cells indicate OSI, characterized by (i) severe disruption/dissolution of all cell membranes, associated with myelin figures and densities, (ii) mitochondrial abnormalities, and (iii) abundant smooth and clathrin-coated vesicles, morphologically resembling coronavirus particles. Ongoing/repeated endothelial cell injury leads to remodeling/multilamellation of the basal laminae in peritubular capillaries.
Multiple factors occurring in COVID-19 viral sepsis likely contribute to OSI, including hyperinflammatory response with monocyte/macrophage recruitment and activation, and hyperferritinemia, all of which are associated with cytokine and free radical storms.
Pathophysiologic overlap exists between sepsis-related AKI in general and COVID-19 AKI, but the OSI in protracted or severe COVID-19 AKI appears significantly more severe.
The OSI mechanism could explain the increased risk of COVID-19 complications in patients with preexisting conditions that are associated with decreased antioxidative defenses.

AKI, acute kidney injury; COVID-19, coronavirus disease 2019; OSI, oxidative stress injury.

abundant cytokines, that cause further host tissue damage. The amplified chain reaction results in the syndrome of viral "sepsis."[7] Morphological studies of AKI in sepsis overall, as well as in hyperinflammatory reactions, needed to validate the preceding hypothesis are, however, very limited.[S22]

The morphological findings in the 2 patients presented here are highly consistent with damage induced by oxidative stress/injury (OSI) secondary to hyperinflammation, in both tubular and endothelial cells. This type of cell injury is characterized by severe, diffuse damage to cellular membranes, leading to microvesiculation and dissolution of the latter, as well as prominent formation of myelin figures. Damage to mitochondrial structure and function is also very characteristic, as is the accumulation of abundant cytoplasmic transport vesicles both clathrin- coated as well as smooth walled.[4,5,S11,S23] Although complement-mediated injury has been proposed to play a role in COVID-19,[S17] we did not observe in these cases morphologically or immunohistochemically typical features associated with complement-mediated cell injury, which is generally characterized by nuclear/cytoplasmic and mitochondrial changes consistent with ion and fluid deregulation, rather than by features of OSI.[S24] Similarly, a significant degree of apoptosis, that is a common form of cell loss in ischemic injury,[S25] was not significant either morphologically or by TUNEL studies.

Tubular cell ultrastructural morphology in these 2 cases was also different from those characterizing the most common forms of acute tubular injury extensively described by Olsen et al.[S26,S27]

Based on these limited studies, we suggest that OSI can play a very significant role in AKI in COVID-19. OSI is a common pathway of cell injury, resulting from a variety of processes, several of which can be identified in systemic viral infection in general, and in COVID-19 specifically.

There appear to be several similarities between overall sepsis-induced AKI and COVID-19 AKI, including early hemodynamic changes, leading to oxidant agent generation, especially in the peritubular capillary microenvironment.[8] Respiratory viruses in general are associated with cytokine production/storm and OSI, leading to cell injury and death,[9] an association that could be relevant in the pathophysiological scenario of sepsis/COVID-19–related AKI.

A dysregulated inflammatory response includes overactivated macrophages and potentially neutrophils, producing a cytokine storm that is followed by a "free radical storm."[S22,S28] Both of our cases, as well as other studies, have shown the prominence of macrophages/monocytes in COVID-19.[S29,S30] Furthermore, alterations in the iron metabolism, including markedly increased serum ferritin that are characteristic of severe COVID-19, also seen in our 2 patients, can contribute to the generation of free radicals and OSI.[S31]

More specifically, hyperferritinemia can lead to widespread tissue injury through massive and uncontrolled activation of T-lymphocytes and of macrophages, followed by excessive production of inflammatory cytokines.[S32,S33] This mechanism is similar to the one of some challenging rheumatic diseases, characterized by hyperferritinemia, high mortality, macrophage activation, and multiple organ dysfunction.[S32] Macrophages can release iron through the action of ferroportin, a process that can be blocked by hepcidin.[S34] Interestingly, hepcidin or hepcidin-like activity is markedly increased in COVID-19, potentially leading to entrapment of iron within cells, particularly macrophages, thus further contributing to the vicious cycle of cytokine-free radical storms.[S31,S34–36] Severe or protracted COVID-19 AKI might be pathophysiologically similar to other entities covered under the general "hyperferritinemic syndrome" umbrella, that also includes septic shock.[S37,S38] The morphological results in the 2 presented cases are different from the typical features of classic acute tubular necrosis (ischemic or toxic), that typically presents with less impressive tubular epithelial cell ultrastructural damage, mainly characterized by diminution of the brush border and basolateral infoldings.[S26,S27] In contrast, the presence of generalized membrane injury, marked mitochondrial changes, and, finally, the prominence of clathrin-coated "viral-like" transport vesicles, are most consistent with OSI. Furthermore, the observed prominent and similar damage in both epithelial and endothelial cell types is a finding that supports a generalized injurious process such as OSI.[4,5,S11,S39–45]

This pathogenetic mechanism has also been implicated in the pathogenesis of sepsis-induced AKI in general, but scarcity of biopsy material in this clinical context has hindered morphological and clinical correlations.[S38] In the COVID-19 AKI context, an additional feature of particular interest, suggesting protracted endothelial injury and repair in the PTC, is the observed multilamellation of the endothelial basal cell lamina, observed in the late biopsy (D84Bx). This change is indicative of repeated endothelial cell injury, regeneration, and repair, and is reminiscent of the PTC response induced from ongoing injury and remodeling seen in antibody-mediated allograft rejection. The OSI pattern of cellular injury is, however, not identified in tubules and endothelium in antibody-mediated rejection,[S46] suggesting a different form of initial insult by a similar repair pathway. The main clinicopathological factors involved in AKI in COVID 19 are summarized in Table 1.

CONCLUSION

The proposed contribution of oxidative stress damage in patients with COVID-19 could account for the increased morbidity and mortality in patients with preexisting conditions (e.g., older age, diabetes, obesity, or hypertension). All of these conditions are characterized by cumulative oxidative damage and weaker defenses against it.[9]

DISCLOSURE

All the authors declared no competing interests.

ACKNOWLEDGMENTS

The authors declare that they have obtained consent from the patients discussed in the report.

SUPPLEMENTARY MATERIALS

Supplementary File (PDF)

Supplementary References.

Figure S1. Additional light microscopy images D10Bx.
Figure S2. Additional light microscopy images D84Bx.
Figure S3. Additional electron microscopy images D84Bx.
Figure S4. Electron micrographs of glomerular tufts.
Figure S5. Hematoxylin-eosin, CD31, CD68, and electron microscopy of ischemic/toxic and sepsis-related AKI without OSI.

REFERENCES

1. Cummings MJ, Baldwin MR, Abrams D, et al. Epidemiology, clinical course, and outcomes of critically ill adults with COVID-19 in New York City: a prospective cohort study. *Lancet*. 2020;395:1763–1770.
2. Su H, Yang M, Wan C, et al. Renal histopathological analysis of 26 postmortem findings of patients with COVID-19 in China. *Kidney Int*. 2020;98:219–227.
3. Smith KD, Akilesh S, Alpers CE, Nicosia RF. Am I a coronavirus? *Kidney Int*. 2020;98:506–507.
4. Castejon O. Ultrastructural pathology of plasma and endoplasmic reticulum membranes of nerve and glial cells: a review. *Biomedical Journal of Scientific & Technical Research*. 2018;10(4).
5. Levine A. Regulation of stress responses by intracellular vesicle trafficking? *Plant Physiology and Biochemistry*. 2002;40:531–535.
6. Menter T, Haslbauer JD, Nienhold R, et al. Postmortem examination of COVID-19 patients reveals diffuse alveolar damage with severe capillary congestion and variegated findings in lungs and other organs suggesting vascular dysfunction. *Histopathology*. 2020;77:198–209.
7. Lin GL, McGinley JP, Drysdale SB, Pollard AJ. Epidemiology and immune pathogenesis of viral sepsis. *Front Immunol*. 2018;9:2147.
8. Wang Z, Holthoff JH, Seely KA, et al. Development of oxidative stress in the peritubular capillary microenvironment mediates sepsis-induced renal microcirculatory failure and acute kidney injury. *Am J Pathol*. 2012;180:505–516.
9. Delgado-Roche L, Mesta F. Oxidative stress as key player in severe acute respiratory syndrome coronavirus (SARS-CoV) Infection. *Arch Med Res*. 2020;51:384–387.